Laminin receptor specific therapeutic gold nanoparticles (^{198}AuNP-EGCg) show efficacy in treating prostate cancer

Ravi Shukla[a], Nripen Chanda[a], Ajit Zambre[a], Anandhi Upendran[b,c], Kavita Katti[a], Rajesh R. Kulkarni[a,d], Satish Kumar Nune[a], Stan W. Casteel[e], Charles Jeffrey Smith[a,f,g], Jatin Vimal[h], Evan Boote[a], J. David Robertson[d,g,i], Para Kan[i], Hendrik Engelbrecht[g], Lisa D. Watkinson[a,f], Terry L. Carmack[a,f], John R. Lever[a,f,j], Cathy S. Cutler[d,g,i,1], Charles Caldwell[k,l,1], Raghuraman Kannan[a,c,1], and Kattesh V. Katti[a,b,c,g,1]

[a]Departments of Radiology and [b]Physics, [d]Nuclear Science and Engineering Institute, [i]Chemistry, [e]Veterinary Pathobiology, [j]Medical Pharmacology and Physiology, [k]Pathology and Anatomical Science, [l]Ellis Fischel Cancer Center, [f]Harry S. Truman Veterans Administration Medical Center, and [g]Missouri University Research Reactor, University of Missouri, Columbia, MO 65212; [c]Nanoparticle Biochem Inc., Columbia, MO 65211; and [h]Shasun Pharmaceuticals Ltd., Guindy, Chennai 600032, Tamil Nadu, India

Edited by* M. Frederick Hawthorne, University of Missouri-Columbia, Columbia, MO, and approved June 25, 2012 (received for review December 23, 2011)

Systemic delivery of therapeutic agents to solid tumors is hindered by vascular and interstitial barriers. We hypothesized that prostate tumor specific epigallocatechin-gallate (EGCg) functionalized radioactive gold nanoparticles, when delivered intratumorally (IT), would circumvent transport barriers, resulting in targeted delivery of therapeutic payloads. The results described herein support our hypothesis. We report the development of inherently therapeutic gold nanoparticles derived from the Au-198 isotope; the range of the ^{198}Au β-particle (approximately 11 mm in tissue or approximately 1100 cell diameters) is sufficiently long to provide cross-fire effects of a radiation dose delivered to cells within the prostate gland and short enough to minimize the radiation dose to critical tissues near the periphery of the capsule. The formulation of biocompatible ^{198}AuNPs utilizes the redox chemistry of prostate tumor specific phytochemical EGCg as it converts gold salt into gold nanoparticles and also selectively binds with excellent affinity to Laminin67R receptors, which are over expressed in prostate tumor cells. Pharmacokinetic studies in PC-3 xenograft SCID mice showed approximately 72% retention of ^{198}AuNP-EGCg in tumors 24 h after intratumoral administration. Therapeutic studies showed 80% reduction of tumor volumes after 28 d demonstrating significant inhibition of tumor growth compared to controls. This innovative nanotechnological approach serves as a basis for designing biocompatible target specific antineoplastic agents. This novel intratumorally injectable ^{198}AuNP-EGCg nanotherapeutic agent may provide significant advances in oncology for use as an effective treatment for prostate and other solid tumors.

nanoradiotherapy | tumor metastases | localized therapy | polyphenols | cellular targeting

Recent data have confirmed that the incidence of prostate cancer is the highest among all estimated new cancer cases in American males, nearly double that of lung cancer (1). Globally, prostate cancer continues to be the second leading cause of cancer-related death in men (1). A detailed study involving 77,000 North Americans has shown that 10 y of regular prostate specific antigen (PSA) screening did not save a significant number of lives (2). Therefore, developments of new therapeutic protocols that provide effective control of the growth and propagation of prostate tumors have gained considerable clinical significance in the care and treatment of prostate cancer patients (3). The latest clinical trials on human prostate cancer patients using various experimental drugs further attest that shrinking prostate tumor sizes led to more than doubled survival in 70–80% of patients with aggressive cancers (3). Although a plethora of therapeutic approaches, which include utility of cytotoxic drugs (paclitaxel, estramustine, carboplatin, and doxorubicin) are currently in clinical practice, unfortunately, none of these chemotherapeutic agents offer a clinically efficient, affordable, and toxicologically safe regimen for effective control of prostate tumors (4, 5). On the radiation induced therapeutic front, the following clinical modalities are at the forefront in prostate tumor therapy: (*i*) intensity-modulated radiation therapy (IMRT), which encounters problems of precise dose delivery and complexity of treatment planning (6); (*ii*) proton therapy, which exploits dose distributions of the Bragg peak effect which has shown some superiority to IMRT, but is hampered by the staggering costs of building and maintaining the facilities (7); (*iii*) stereotactic body radiotherapy (SBRT) for early-stage prostate cancer treatment, which exploits the alpha/beta ratio typical of slow growing malignancies, diminishes the volume of rectum and bladder irradiated during conformal therapy, but shows only an average of 20% decrease in prostate tumor volume (8); (*iv*) Brachy therapy, which uses iodine-125 or palladium-103 radioactive seeds and Y-90 immobilized glass microspheres (Therasphere™), have drawbacks associated with limited retention of therapeutic payloads and also result in significant leakage from tumor sites because of size differentials (9). The brachy seeds are in the 50–100 micron size range whereas tumor vasculature allows 150–300 nm, thereby prohibiting effective penetration of radioactive seeds within prostate tumor vasculature and consequently minimizing therapeutic payloads at tumor sites; and (*v*) External Beam Radiation Therapy (EBRT), which is being used for androgen ablation has shown an average 20% decrease in prostate tumor volume (10).

Radioactive nanotechnology is poised to play a pivotal role in molecular imaging and therapy of cancers because inherently therapeutic nanoparticles can be created and designed to match the sizes of tumor vasculature so that optimal therapeutic payloads with minimum leakage away from target sites can be achieved (11, 12). Nanoscale imaging agents, tumor specific nanosensors, and highly effective therapeutic nanoprobes, derived from radioactive metallic nanoparticles and engineered nanomaterials, have already demonstrated "proof of concept" for diagnosis, imaging and treatment of many cancers at the cellular and molecular levels (13, 14). While specific nanoparticles can indivi-

Author contributions: C.S.C., C.C., R.K., and K.V.K. designed research; R.S., A.Z., K.K., R.R.K., C.J.S., E.B., J.D.R., P.K., H.E., L.D.W., T.L.C., J.R.L., and C.S.C. performed research; A.Z., S.K.N., and S.W.C. contributed new reagents/analytic tools; R.S., N.C., A.Z., A.U., C.J.S., J.V., E.B., J.R.L., C.S.C., C.C., R.K., and K.V.K. analyzed data; and R.S., N.C., A.U., J.R.L., C.S.C., C.C., and K.V.K. wrote the paper.

The authors declare no conflict of interest.

*This Direct Submission article had a prearranged editor.

[1]To whom correspondence may be addressed. E-mail: KattiK@health.missouri.edu or KannanR@health.missouri.edu or CutlerC@missouri.edu or CaldwellC@health.missouri.edu.

This article contains supporting information online at www.pnas.org/lookup/suppl/doi:10.1073/pnas.1121174109/-/DCSupplemental.

www.pnas.org/cgi/doi/10.1073/pnas.1121174109

dually act as imaging or therapy agents, radioactive gold nanoparticles will provide unprecedented dual imaging and therapeutic ("theranostic") capabilities for use in the development of a new generation of cancer diagnostic and therapeutic agents (15–19).

We envisioned that radioactive gold nanoparticles, which are inherently therapeutic, present realistic prospects in achieving optimal therapeutic payloads in prostate tumors because of their (*i*) size, (*ii*) inherent affinity toward tumor vasculature, and (*iii*) most importantly, their favorable radiochemical properties (19–21). Au-198 provides a desirable beta energy emission and half-life that destroys tumor cells/tumor tissue ($\beta_{max} = 0.96$ MeV; half-life of 2.7 d) (18). Its penetration range (up to 11 mm in tissue or up to 1100 cell diameters) is sufficiently long to provide cross-fire effects to destroy prostate tumor cells, but short enough to minimize radiation exposure to tissues near the capsule periphery. Our approach to achieving tumor specificity and optimal retention of therapeutic payloads of radioactive gold nanoparticles at prostate tumor sites has involved surface conjugation of radioactive gold nanoparticles with epigallocatechin-gallate (EGCg). EGCg is a major phytochemical component of green tea and has been used for a long time as a food supplement because of its strong antioxidant properties. Extensive in vitro and in vivo investigations have provided credible evidence to demonstrate that EGCg, along with other flavonoids, can be beneficial in treating brain, prostate, cervical and bladder cancers (22–24). We hypothesized that the redox properties of EGCg (comprised of polyphenolic constitution) could be effectively utilized as a reducing agent to convert radioactive gold precursor to radioactive gold nanoparticles—through a 100% biocompatible nanotechnological process without the intervention of any toxic chemical (25).

An additional advantage of EGCg is its ability to target Laminin receptor (Lam 67R), which is over expressed on human prostate cancer cells (26). Lam 67R is a 67 kDa cell surface protein, first isolated as a non-integrin high affinity laminin binding protein from murine cancer cells in 1983 by two independent research groups (27, 28). EGCg has been known to bind to Lam 67R with excellent specificity and selectivity (26). Therefore, we also postulated that the utility of EGCg coating over gold nanoparticles would serve additional targeting features through its capabilities to internalize into prostate tumor cells via Lam 67R receptors. The fabrication of EGCg functionalized radioactive gold nanoparticles (^{198}AuNP-EGCg) in our laboratory may be considered a genesis for realistic applications of prostate tumor receptor specific diagnosis and therapy.

In this paper, we present experimental results that validate our hypothesis and also present full details encompassing: (*i*) synthesis and complete characterization of EGCg functionalized radioactive gold nanoparticles, (*ii*) experimental results on prostate tumor specificity of AuNP-EGCg through in vitro Lam 67R binding assays, (*iii*) evidence of endocytosis due to Laminin receptors on prostate tumor cells and quantitative estimation of AuNP-EGCg within PC-3 cells using neutron activation analysis (NAA), and (*iv*) therapeutic efficacy studies of ^{198}AuNP-EGCg in prostate tumor bearing mice, demonstrating excellent tumor retention resulting in over 70% inhibition of tumor growth through singular intratumoral injection. The overall oncological implications and clinical potential of this new nano therapeutic agent in treating human prostate and various other solid tumors are discussed.

Results and Discussion

Current chemo and radiopharmaceutical approaches do not control prostate tumor growth effectively because of inefficiencies associated with limited retention of therapeutic payloads within tumor sites. We therefore challenged ourselves to develop a radioactive gold nanoparticulate construct, capable of penetrating tumor vasculature, to achieve optimum therapeutic payloads—an approach, if successful, that would effectively treat prostate tumors without toxic side effects. We sought nothing less than a significant oncological breakthrough for treating prostate cancer, using a readily injectable 'non seed' radioactive nanotherapeutic agent, ^{198}AuNP-EGCg, produced using a FDA approved phytochemical, EGCg. This phytochemical serves multiple important roles as: (*i*) a nanoparticle initiator, (*ii*) a surface stabilizer via coating of EGCg polyphenols on gold nanoparticles, and most importantly (*iii*) a provider of a non toxic prostate tumor specific EGCg Lam receptor targeting agent capable of forming in vivo stable bonds on the surface of radioactive gold nanoparticles. Through our discovery of this novel "Trojan Horse" approach, we have achieved optimum therapeutic payloads at prostate tumor sites and have shown therapeutic efficacy in reducing prostate tumor volumes in tumor bearing mice as outlined in the following sections.

Synthesis and Characterization of EGCg-AuNP. We initially synthesized the non-radioactive surrogate EGCg-AuNP by simple mixing of sodium tetrachloroaurate ($NaAuCl_4$) with (-)(EGCg) in deionized water (Scheme 1). In this reaction, we utilized the strong chemical reduction properties of EGCg to convert gold salt into gold nanoparticles without the intervention of any toxic chemical. The redox potential of $AuCl_4^-$/Au [+0.99 V vs. Standard Hydrogen Electrode (SHE)] is significantly positive as compared to the redox potential of EGCg (+0.42 V vs. SHE), resulting in a thermodynamically feasible redox couple of $AuCl_4^-$/EGCg, leading to the reduction of $AuCl_4^-$ by EGCg to form gold nanoparticles. The full details on physicochemical characterization, robust in vitro and in vivo stability, and hemocompatibility assessment of EGCg-AuNP, are described in the *SI Text*, Figs. S1–S3 respectively.

Synthesis and Characterization of Radioactive ^{198}AuNP-EGCg Therapeutic Agent. The radioactive ^{198}AuNP-EGCg was synthesized adopting the same protocol optimized for the non-radioactive surrogate, except that the radioactive tetrachloroauric acid ($H^{198}AuCl_4$) was used in carrier $NaAuCl_4$ solution and the solution was brought to pH 7 and made isotonic using NaOH and Delbecco's phophate buffered saline. The UV-Vis spectrum of ^{198}AuNP-EGCg correlated well with the spectroscopic features observed for the non-radioactive EGCg-AuNP surrogate (at approximately 535 nm), indicating similarity of nanoparticulate species at the tracer and macroscopic levels. Radio-TLC confirmed the formation of ^{198}AuNP-EGCg in ≥99% yields, proving the extraordinary reduction capabilities of EGCg even at tracer levels (*SI Text*, Fig. S4).

Laminin 67 Receptor Mediated Cellular Internalization of EGCg-AuNP. Of significance in conjugating EGCg over AuNPs has been to render targeting capabilities of EGCg-AuNP toward the laminin

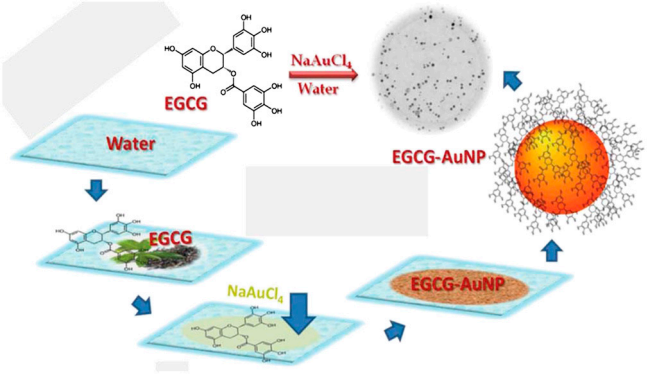

Scheme 1. Schematic presentation of the synthesis of EGCg-AuNP.

receptors (Lam 67R), which are over expressed on human prostate cancer cells (26). In order to prove the affinity of the EGCg-AuNP nanoconstruct toward Lam 67R receptors, qualitative and quantitative prostate cancer receptor binding assays were performed. Laminin 67R is a 67 kDa cell surface protein and its expression has been correlated with aggressiveness and metastatic behavior of a variety of cancers including prostate, breast, and colon cancer (29–34). Additionally, it has been shown that suppression of the expression of the precursor of Lam 67R (37LBP) using siRNA techniques leads to inhibition of lung cancer cell proliferation in vitro and tumor formation in vivo, clearly indicating the role of Lam 67R in tumorigenicity (35). Studies by Tachibana et al. have shown that EGCg binds to Lam 67R in prostate cancer cells in a concentration dependent manner (26). It is therefore reasonable to hypothesize that EGCg-AuNP internalization in prostate cancer cells (PC-3) through endocytosis will be mediated through Lam 67R receptor expression. In order to investigate this possibility, we have monitored the level of Lam 67R expression on PC-3 cells through quantitative RT-PCR and confocal microscopy using $MLuC_5$ antibody as a probe (Fig. 1*C* and Fig. S5). A detailed analysis of Lam 67R expression in PC-3 cells revealed that a majority of cells expressed Lam 67R transcripts at mRNA levels and are also immunoreactive to the $MLuC_5$ antibody, thereby confirming the expression of Lam 67R at transcriptional as well as at post translational levels. After confirming this expression, the PC-3 cells were exposed to various concentrations of EGCg-AuNP. These experiments revealed that a significant amount of EGCg-AuNPs were internalized in PC-3 cells and localized in vacuoles as well as in the cytoplasm without disturbing the nucleus (Fig. 1 *A* and *D*). The dark field microscopic image depicts the visual observation of PC-3 cells following EGCg-AuNP treatment (Fig. 1*D*). The internalized nanoparticles are found intact with clear boundaries, confirming high in vitro and in vivo stability of EGCg-AuNPs (Fig. 1*B*). The highly efficient cellular uptake of EGCg-AuNPs demonstrates the Lam67R receptor affinity and validates our hypothesis on the creation of prostate tumor specific gold nanoparticles via surface functionalization with EGCg that results in a "Trojan Horse" like uptake.

In order to gain further insights on the receptor specific binding affinity, we have performed receptor blocking studies with laminin, the natural ligand for the receptor or Lam 67R specific $MLuC_5$ antibody. Lam 67R receptors were blocked by pretreatment of PC-3 cells with laminin, followed by a 90 min incubation with EGCg-AuNPs. The color of the PC-3 cellular pellets turned dark red [Fig. 1*F* (pellets 1, 2)], when they were not pretreated with laminin, indicating a maximum level of EGCg-AuNP internalization. A decrease in the intensity of the red color in PC-3 cellular pellets pretreated with laminin indicates significantly reduced endocytosis [Figs. 1*E* and 2*F* (pellets 3 and 4)]. Additional proof that the internalization of EGCg-AuNPs within PC-3 cells is mediated by Lam 67R expression came from receptor saturation experiments using Lam 67R specific $MLuC_5$ anti-

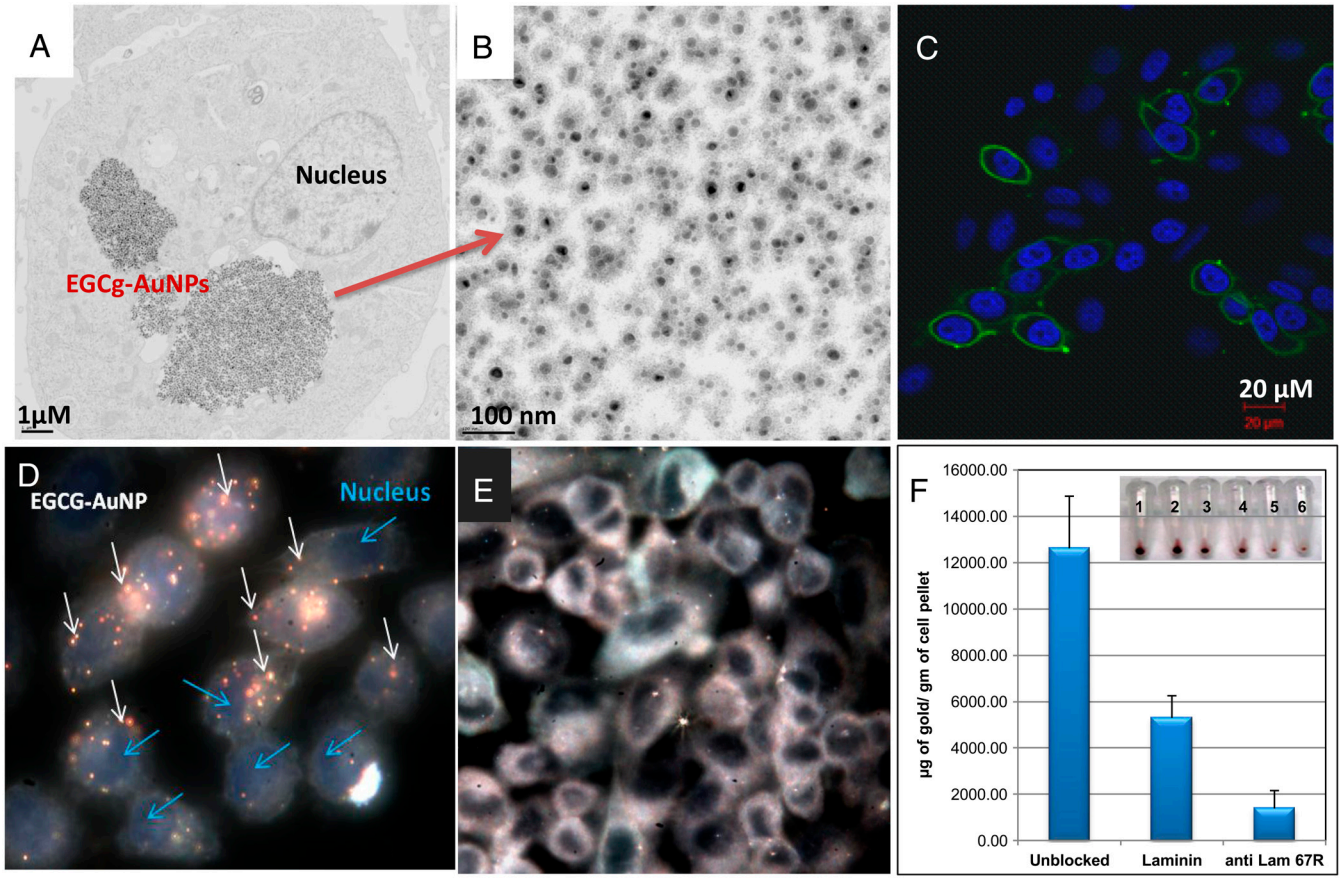

Fig. 1. EGCg-AuNP in PC-3 cells over expressing Lam 67R. (*A*) TEM image showing internalization of nanoparticles 4 h post treatment; (*B*) high magnification TEM image showing intact EGCg-AuNP inside PC-3 cells; (*C*) confocal microscopic image showing immunocytochemical localization of Lam 67R in PC-3 cells (the nuclei were stained with DAPI); (*D*) dark field image showing nanoparticle uptake 4 h post treatment; (*E*) inhibition in particle uptake in the presence of Laminin 67 receptor blocking antibody; and (*F*) quantitative uptake analysis of EGCg-AuNP in PC-3 cells as measured by neutron activation analysis. The cells were pre-incubated either with Laminin or with Lam67R antibody or no pretreatment followed by 90 min incubation with 30 µg of EGCg-AuNP. The cells were washed extensively and subjected to neutron activation analysis. *Inset* in (*F*) represents the visual color of the pellet without any pretreatment (1, 2), with laminin (3, 4) and Lam 67R (5, 6) antibody pretreated cells.

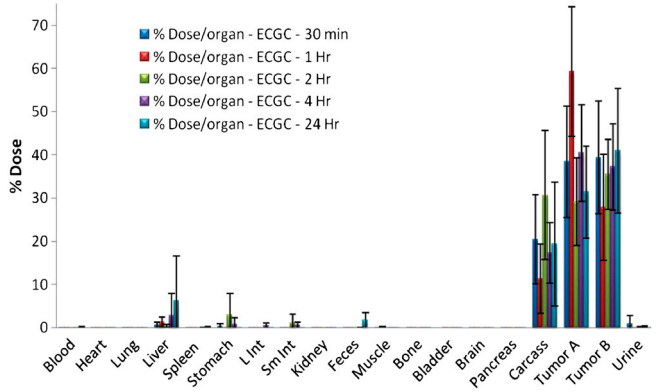

Fig. 2. Retention of radioactivity in tumors following intra-tumoral injection of ^{198}AuNP-EGCg in mice ($n = 5$, means ± SD).

body. In this experiment, Lam 67 receptors were saturated by pre incubating PC-3 cells with $MLuC_5$ antibody (4 μg/mL). Subsequently, these cells were incubated with a large excess of EGCg-AuNP. Saturation of Lam 67R with $MLuC_5$ antibody resulted in a significantly reduced internalization of EGCg within PC-3 cells with consequent reduction in the intensity of the color of the pellets [Fig. 1*F* (pellets 5 and 6)]. The results from the above experiments, as depicted in graphical sketches in Fig. 1, infer that blocking Lam 67R on PC-3 cells either through the laminin or $MLuC_5$ antibody results in saturation of receptors with a concomitant decrease in the internalization of EGCg-AuNP. In order to estimate gold content within PC-3 cells, pre and post treatment with laminin or $MLuC_5$ antibody, we have further performed quantitative estimation of gold concentrations within samples of PC-3 cells using neutron activation analysis (NAA). It should be noted that NAA measurements estimate the amount of gold in a cell pellet sample and provide the most accurate quantification of the total amount of gold internalized within the cells, allowing direct measurement of cellular uptake of AuNPs. NAA analysis (Fig. 1*F*) clearly showed a marked decrease in the amount of gold content in PC-3 cells that were pretreated with laminin or $MLuC_5$ antibody as compared with control cells. Blocking of Lam 67R by presaturation either with Lam-67R or $MLuC_5$ antibody on PC-3 cells resulted in significant reduction of gold concentration (approximately 60% and 85%, respectively, relative to control cells) in cellular pellets. Therefore, our detailed studies on the qualitative and quantitative estimation of gold content in PC-3 cell samples have established that the uptake of EGCg-AuNPs within PC-3 cells is mediated through Lam 67R and present opportunities for the selective uptake of therapeutic gold nanoparticles within prostate tumors. Excellent retention of therapeutic payloads of ^{198}AuNP-EGCg within prostate tumors in mice were attributed to the high affinity of the EGCg functionalized gold nanoparticles toward Laminin receptors (*SI Text*). These encouraging data led us to perform detailed therapeutic efficacy studies of ^{198}AuNP-EGCg and the details are described below.

Pharmacokinetics and Tumor Retention of ^{198}AuNP-EGCg. Pharmacokinetic properties of ^{198}AuNP-EGCg have been investigated in detail as they relate to retention of therapeutic payloads within prostate tumors. The tumor selectivity and retention of Au-198 beta emitting radioactivity are important in achieving maximum therapeutic efficacy with minimal side effects. In order to achieve maximum therapeutic efficacy, several factors including the size, stability of nanoparticles in the tumor microenvironment, ability of nanoparticles to interact with cells and efficient cellular internalization through active targeting, must all operate in synergy. Our studies have confirmed that over 70% of the injected dose of ^{198}AuNP-EGCg is retained within prostate tumors up to 24 h (Fig. 2, *SI Text*). There is minimum leakage of injected dose in to non-target organs and blood. As reported in the literature, nanoparticles with a hydrodynamic diameter size of 80 nm and above are cleared in vivo by reticuloendothelial system (RES) organs (36). Our pharmacokinetic data confirm that small amounts of dose leaked from the tumor are cleared by RES uptake and minimal renal clearance is observed.

Therapeutic Efficacy Studies of ^{198}AuNP-EGCg. We have used a unilateral flank model of prostate cancer derived from human PC-3 cells in SCID mice model, a promising platform for prostate cancer (37–40).

The results from the single-dose radiotherapy study of ^{198}AuNP-EGCg in human prostate cancer bearing SCID mice are shown in Fig. 3. Within one week after administration of ^{198}AuNP-EGCg (Day 14, 136 μCi), tumor growth in the treated animals appeared to be slowing with respect to controls. By two weeks after ^{198}AuNP-EGCg administration (Day 18), tumor volumes were four-fold lower ($p = 0.04$) for treated animals as compared to the control group. This significant therapeutic effect was maintained throughout the five week study. By three weeks after ^{198}AuNP-EGCg administration (Day 28), tumor volumes for the control animals were five-fold greater with respect to those for the radiotherapy group ($p = 0.01$; 0.28 ± 0.08 vs. 0.05± 0.02 cm^3, means ± sem). No significant differences were noted between the DPBS controls and animals treated with EGCg alone in DPBS solutions, demonstrating that EGCg in itself did not have any therapeutic effect at this dosage level. After evaluation on Day 21, one animal from each of the EGCg and the DPBS control groups was terminated because of excessive weight loss (>20%). Two additional animals from the EGCg group were terminated due to weight loss on Day 25, and one animal from the ^{198}AuNP-EGCg group was terminated because of weight loss on Day 39. Studies of the EGCg ($n = 4$) and DPBS control ($n = 6$) groups were concluded on Day 28 due to increasing tumor burdens.

The end-of-study biodistribution on Day 42 showed that 37.4. ± 8.1 %ID of ^{198}AuNP-EGCg (mean ± sem; $n = 5$) remained in the residual tumor, while 17.8. ± 6.1 %ID was noted for carcass and 2.5. ± 1.7 %ID was observed in the liver. Retention in other tissues was negligible, with radioactivity near background levels for blood, heart, lung, spleen, intestines, stomach, bone, brain and skeletal muscle.

Blood parameters within the tumor-bearing EGCg and ^{198}AuNP-EGCg treatment groups, as well as the DPBS controls, showed no significant differences between groups (ANOVA) from each other, or with baseline levels from a fourth group

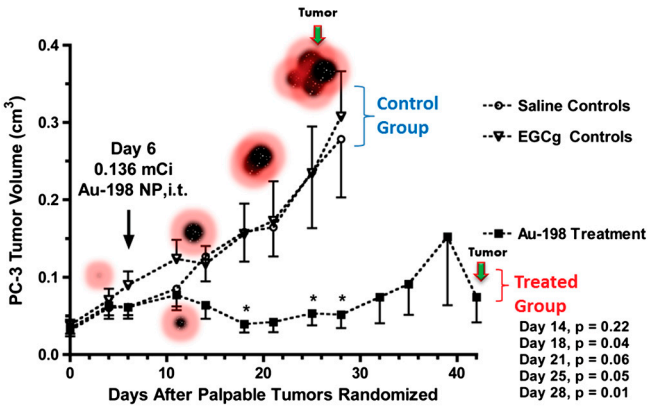

Fig. 3. Therapeutic efficacy of EGCg-AuNPs after a single-dose intra-tumoral administration of ^{198}AuNP-EGCg in human prostate cancer-bearing SCID mice (means ± SEM). By Day 18, treated animal tumors were four-fold smaller ($p = 0.04$) than those for EGCg treated or saline control animals. The therapeutic effect was maintained over a five week period.

of SCID mice that had not been experimentally manipulated. Comparisons included mean counts for white cells, red cells and lymphocytes, as well as hemoglobin and total protein concentrations (Fig. S6, *SI Text*). We did not attempt to detect the ow level (<1.0 ng/mouse) of stable Hg-198 that would result from decay of the Au-198 therapy dosage (136 μCi). There were no clinical signs of toxicity, and blood measures of the ^{198}AuNP-EGCg treated animals indicate that the radiotherapy was not only highly effective, but well tolerated. These findings indicate that the Laminin receptor specific EGCg functional unit used to coat and stabilize the AuNPs has an important role in determining in vivo stability, tumor selectivity, and tissue distribution profile (41). The importance of the EGCg coating is evident by comparing the retention and therapeutic efficacy data to data from our previously reported (18) gum arabic stabilized radioactive gold nanoparticles (GA-^{198}AuNP). Gum Arabic is a glycoprotein and is not known to have affinity towards Lam-67R receptor present in prostate tumor cells, and therefore, GA-^{198}AuNP serves as an excellent control agent for comparison of in vivo therapeutic efficacy characteristics with those of ^{198}AuNP-EGCg. The % ID/g of retention of therapeutic payloads, for the GA-^{198}AuNP agent (75% ID/g) and ^{198}AuNP-EGCg agent (200% ID/g), 24 h post intratumoral injection, showed a marked difference (Fig. S7, *SI Text*) between the two agents. This significantly longer retention of ^{198}AuNP-EGCg within the tumor allowed us to inject only a third of the activity (136 μCi for ^{198}AuNP-EGCg vs 408 μCi for GA-^{198}AuNP) and yet achieve comparable tumor volume reduction with time. These data provide evidence for the requirement of EGCg coating on the radioactive gold nanoparticles to achieve effective cellular retention and therapeutic delivery at the tumor site.

Localized Therapy May Achieve Deceleration of Metastases. The propensity with which EGCg-AuNPs internalize within PC-3 cells is evidenced by the high density of nanoparticles within prostate tumor cells as depicted in the TEM images shown in Fig. 1*A*. These results fully corroborate the receptor mediated internalization studies as discussed above (Fig. 1 *D–F*). It is important to recognize that the identity of nanoparticles within PC-3 cells is maintained as there are no aggregated domains of gold nanoparticles within the PC-3 cells (Fig. 1*B*). As discussed in the therapeutic efficacy studies section, intratumoral delivery of ^{198}AuNP-EGCg nanoparticles within prostate tumors in mice resulted in effective control of tumor growth. The retention of over 70% of the injected dose of ^{198}AuNP-EGCg within tumor sites and its consequent influence in achieving excellent therapeutic efficacy is shown in Figs. 2 and 3. Therefore, the 'ultra efficient' entry of EGCg-AuNPs across prostate tumor cell membranes has the potential to effectively destroy tumor cells within localized areas. This will prevent cell propagation and recruitment of tumor cells (and stem tumor cells) into bone marrow—a pathway to decelerate and stop metastases of prostate and other solid tumors.

Conclusions

Interaction of biocompatible EGCg with ^{198}Au precursor affords the production of inherently therapeutic gold nanoparticles through a novel synthetic route, effectively eliminating toxic chemicals that are routinely utilized in pharmaceutical formulations. Toxicity of species from radioactive decay are important considerations in the ultimate clinical translation of ^{198}AuNP-EGCg for human use. The final decay product of Au-198 is Hg-198, a stable isotope. Therapeutic applications of radioactive colloidal gold in radiation synovectomy and in related clinical use in human patients are prevalent in the literature and the toxicity effects due to radioactive decay of Au-198 to mercury have been pronounced insignificant at the therapeutic dose of administration (42). A major advantage of such radiotherapy is that only small amounts of radioactivity are required for imaging and therapy (43). The amount of stable mercury produced by decay is low such that no toxicity should be observed. For instance, decay of a 20 mCi injected dose of Au-198 would result in 80 ng of Hg. Considering that the EPA approved toxicity levels of Hg in humans is about 5.8 μg/L of blood, if we assume that all the Hg that is produced leaks out in to the blood, the total amount of Hg produced from the Au-198 decay will result in a concentration of 16 ng/L Hg. This amount is 1,000 fold lower than the safety margin provided by the EPA (http://www.epa.gov/hg/exposure.htm#elem) for the typical dose that would be administered in the clinic (44). Therefore, toxicity of Hg will not be an impediment in the clinical applications of ^{198}AuNP-EGCg in treating various different forms of human cancers. The retention of over 70% of the injected dose of ^{198}AuNP-EGCg within tumor sites and its consequent influence in achieving excellent therapeutic efficacy (as shown in Figs. 2 and 3) provides potential for the nanotherapeutic agent to become a useful tool in treating prostate cancer over the conventional chemotherapy or radiotherapeutic approaches (45–47).

Materials and Methods

Synthesis and Characterization of ^{198}AuNP-EGCg and its Non-Radioactive Surrogate EGCg-AuNP. ^{198}AuNP-EGCgs were synthesized by stirring aqueous solutions of EGCg and radioactive tetrachloroauric acid H^{198}AuCl$_4$ [University of Missouri Research Reactor (MURR)]. The color of the mixture turned purple-red from pale yellow within 5 min and the formation of gold nanoparticles was characterized by UV-Visible spectroscopy. Full details of synthesis, characterization and stability studies of EGCg-AuNP in biologically relevant solutions (10% NaCl, 0.5% cysteine, 0.2 M histidine, 0.5% HSA and different pH buffers) (7, 9) are provided in *SI Text* (15).

Therapeutic Efficacy Studies. A colony of 21 female SCID mice bearing PC-3 tumors from cell passage 21 was established as described in *SI Text*, except a unilateral right flank model was employed, and animals received ear tag identifiers while under inhalational anesthesia. Solid tumors developed over a period of 22 d, and animals were then randomized (denoted Day 0) into a control and two treatment groups ($n = 7$) having no significant differences (ANOVA) in tumor volumes ($p = 0.69$) or body weights ($p = 0.23$) between groups. Tumor volumes were determined by caliper measurements using the formula $V = \text{length} \times \text{width} \times \text{depth}$. Group mean tumor volumes ranged from 0.031–0.041 cm^3, while group mean body weights ranged from 22.6–24.0 g. Under inhalational anesthesia on Day 6, one treatment group received ^{198}AuNP-EGCg (136 μCi) in DPBS (30 μL, *i.t.*) while the second treatment group received the non-radioactive EGCg formulation in DPBS (30 μL, *i.t.*). The control group received only DPBS (30 μL, *i.t.*). On the day of treatment, one animal in the ^{198}AuNP-EGCg group displayed a tumor volume that was two standard deviations above the group mean, and near the critical score for an outlier using the Grubbs' test. This animal was removed from further analysis, leaving an ^{198}AuNP-EGCg group ($n = 6$) that showed no significant difference ($p = 0.69$; ANOVA) in tumor volumes with the non-radioactive EGCg and DPBS control groups ($n = 7$) on Day 6.

Overall health evaluations, including measurements of tumor volumes and body weights, were conducted twice each week. End of study for the ^{198}AuNP-EGCg treatment group was on Day 42. These animals ($n = 5$) were euthanized by cervical dislocation, and blood samples were collected by cardiac puncture and treated as described *SI Text*. Samples of tumor, carcass and organs of interest were harvested, weighed and counted for radioactivity in comparison to a sample of the injected dose using an automated γ-counter. Blood values were compared (ANOVA) to those from fresh bloods obtained from a separate group of female ICRSC-M SCID mice ($n = 7$) that received no experimental manipulations, and were maintained through the end of the study.

ACKNOWLEDGMENTS. Authors wish to thank Dr. R. R. Bhonde of National Centre for Cell Science, India for the help in completing hemocompatibilty studies. This work has been supported by grants from the National Institute of Health/National Cancer Institute under the Cancer Nanotechnology Platform Program (Grant no.: 5R01CA119412-01, and NIH-1R21CA182460-01). The authors (RK and KVK) thank Shasun-NBI Inc and Shasun Pharmaceuticals India for developmental funding in the EGCg-AuNP project.

1. American Cancer Society (2010) *Cancer Facts and Figures 2010* (American Cancer Society, Atlanta), pp 23–35.
2. Schröder FH, et al. (2009) Screening and prostate-cancer mortality in a randomized European study. *N Engl J Med* 360:1320–1328.
3. Abouassaly R, Paciorek A, Ryan CJ, Carroll PR, Klein EA (2009) Predictors of clinical metastasis in prostate cancer patients receiving androgen deprivation therapy: Results from CaPSURE. *Cancer* 115:4470–4476.
4. Urakami S, et al. (2002) Combination chemotherapy with paclitaxel, estramustine and carboplatin for hormone refractory prostate cancer. *J Urol* 168:2444–2450.
5. Millikan R, et al. (2003) Randomized, multicenter, phase II trial of two multicomponent regimens in androgen-independent prostate cancer. *J Clin Oncol* 21:878–883.
6. Lu R, et al. (2008) Reduced-order constrained optimization in IMRT planning. *Phys Med Biol* 53:6749–6766.
7. Terasawa T, et al. (2009) Systematic review: Charged-particle radiation therapy for cancer. *Ann Intern Med* 151:556–565.
8. Katz AJ, Santoro M, Ashley R, Diblasio F, Witten M (2010) Stereotactic body radiotherapy for organ-confined prostate cancer. *BMC Urol* 10:1.
9. Wollner I, et al. (1998) Effects of hepatic arterial yttrium 90 glass microspheres in dogs. *Cancer* 61:1336–1344.
10. Richaud P, et al. (1998) Clinical and biological evaluation of the response to neoadjuvant hormone therapy before radiotherapy in nonmetastatic cancers of the prostate. *Cancer Radiother* 2:27–33 (in fre).
11. Bouchat V, et al. (2010) Radioimmunotherapy with radioactive nanoparticles: Biological doses and treatment efficiency for vascularized tumors with or without a central hypoxic area. *Med Phys* 37:1826–1839.
12. Mironidou-Tzouveleki M, Tsartsalis S (2010) Nanotechnology and radiopharmaceuticals: Diagnostic and therapeutic approaches. *Curr Drug Deliv* 7:168–174.
13. Matson JB, Grubbs RH (2008) Synthesis of fluorine-18 functionalized nanoparticles for use as in vivo molecular imaging agents. *J Am Chem Soc* 130:6731–6733.
14. Xie H, Wang ZJ, Bao A, Goins B, Phillips WT (2010) In vivo PET imaging and biodistribution of radiolabeled gold nanoshells in rats with tumor xenografts. *Int J Pharm* 395:324–330.
15. Kattumuri V, et al. (2007) Gum arabic as a phytochemical construct for the stabilization of gold nanoparticles: In vivo pharmacokinetics and X-ray-contrast-imaging studies. *Small* 3:333–341.
16. Kannan R, et al. (2012) Functionalized radioactive gold nanoparticles in tumor therapy. *Wiley Interdiscip Rev Nanomed Nanobiotechnol* 4:42–51.
17. Kannan R, et al. (2006) Nanocompatible chemistry toward fabrication of target-specific gold nanoparticles. *J Am Chem Soc* 128:11342–11343.
18. Chanda N, et al. (2010) Radioactive gold nanoparticles in cancer therapy: Therapeutic efficacy studies of GA-^{198}AuNP nanoconstruct in prostate tumor-bearing mice. *Nanomedicine* 6:201–209.
19. Balogh L, et al. (2007) Significant effect of size on the in vivo biodistribution of gold composite nanodevices in mouse tumor models. *Nanomedicine* 3:281–296.
20. Chanda N, et al. (2010) Bombesin functionalized gold nanoparticles show in vitro and in vivo cancer receptor specificity. *Proc Natl Acad Sci USA* 107:8760–8765.
21. Chanda N, et al. (2011) An effective strategy for the synthesis of biocompatible gold nanoparticles using cinnamon phytochemicals for phantom CT imaging and photoacoustic detection of cancerous cells. *Pharm Res* 28:279–291.
22. Johnson JJ, Bailey HH, Mukhtar H (2010) Green tea polyphenols for prostate cancer chemoprevention: A translational perspective. *Phytomedicine* 17:3–13.
23. Khan N, Adhami VM, Mukhtar H (2009) Review: Green tea polyphenols in chemoprevention of prostate cancer: Preclinical and clinical studies. *Nutr Cancer* 61:836–841.
24. Qiao Y, Cao J, Xie L, Shi X (2009) Cell growth inhibition and gene expression regulation by (-)-epigallocatechin-3-gallate in human cervical cancer cells. *Arch Pharm Res* 32:1309–1315.
25. Faraday M (1857) Experimental relations of gold (and other metals) to light. *Phil Trans R Soc Lond* 147:145–181.
26. Tachibana H, Koga K, Fujimura Y, Yamada K (2004) A receptor for green tea polyphenol EGCG. *Nat Struct Mol Biol* 11:380–381.
27. Rao NC, Barsky SH, Terranova VP, Liotta LA (1983) Isolation of a tumor cell laminin receptor. . *Biochem Biophys Res Commun* 111:804–808.
28. Malinoff HL, Wicha MS (1983) Isolation of a cell surface receptor protein for laminin from murine fibrosarcoma cells. *J Cell Biol* 96:1475–1479.
29. Castronovo V, et al. (1992) Inverse modulation of steady-state messenger RNA levels of two non-integrin laminin-binding proteins in human colon carcinoma. *J Natl Cancer Inst* 84:1161–1169.
30. Castronovo V, et al. (1990) Immunodetection of the metastasis-associated laminin receptor in human breast cancer cells obtained by fine-needle aspiration biopsy. *Am J Pathol* 137:1373–1381.
31. Cioce V, et al. (1991) Increased expression of the laminin receptor in human colon cancer. *J Natl Cancer Inst* 83:29–36.
32. Martignone S, et al. (1993) Prognostic significance of the 67-kilodalton laminin receptor expression in human breast carcinomas. *J Natl Cancer Inst* 85:398–402.
33. Pellegrini R, Martignone S, Menard S, Colnaghi MI (1994) Laminin receptor expression and function in small-cell lung carcinoma. *Int J Cancer Suppl* 8:116–120.
34. Basolo F, et al. (1996) Expression of the Mr 67,000 laminin receptor is an adverse prognostic indicator in human thyroid cancer: An immunohistochemical study. *Clin Cancer Res* 2:1777–1780.
35. Satoh K, et al. (1999) Diminution of 37-kDa laminin binding protein expression reduces tumour formation of murine lung cancer cells. *Br J Cancer* 80:1115–1122.
36. Zhang G, et al. (2009) Influence of anchoring ligands and particle size on the colloidal stability and in vivo biodistribution of polyethylene glycol-coated gold nanoparticles in tumor-xenografted mice. *Biomaterials* 30:1928–1936.
37. Valkenburg KC, Williams BO (2011) Mouse models of prostate cancer. *Prostate Cancer* 895238.
38. Shen MA-S, Abate-Shen C (2010) Molecular genetics of prostate cancer: New prospects for old challenges. *Genes Dev* 24:1967–2000.
39. Pang X, et al. (2011) (-)-Gossypol suppresses the growth of human prostate cancer xenografts via modulating VEGF signaling-mediated angiogenesis. *Mol Cancer Ther* 10:795–805.
40. Bauerschlag DO, et al. (2010) Sunitinib (SU11248) inhibits growth of human ovarian cancer in xenografted mice. *Anticancer Res* 30:3355–3360.
41. Fent GM, et al. (2009) Biodistribution of maltose and gum arabic hybrid gold nanoparticles after intravenous injection in juvenile swine. *Nanomedicine* 5:128–135.
42. Van Soesbergen RM, Hoefnagel CA, Marcuse HR, Dijkstra PF, Bernelot Moens HJ (1988) Radiosynoviorthesis of the knee: A doubleblind trial of 1 versus 5 mCi Gold-198. *Clin Rheumatol* 7:224–230.
43. Bhattacharyya S, Dixit M (2011) Metallic radionuclides in the development of diagnostic and therapeutic radiopharmaceuticals. *Dalton Trans* 40:6112–6128.
44. Pagnanelli RA, Basso DA (2010) Myocardial perfusion imaging with 201Tl. *J Nucl Med Technol* 38:53–60.
45. Begg AC, Stewart FA, Vens C (2011) Strategies to improve radiotherapy with targeted drugs. *Nat Rev Cancer* 11:239–253.
46. Hoppe R, and PTLRM (2010) *Leibel and Phillips Textbook of Radiation Oncology* (Elsevier, New York), 3rd Ed.
47. Bhide SA, Nutting CM (2010) Recent advances in radiotherapy. *BMC Med* 8:25.